d-PCL(530)/siloxane biohybrid films doped with protic ionic liquids

M. Fernandes[a,b], M. A. Cardoso[a,c], L. C. Rodrigues[d], M. M. Silva[e], R. A. S. Ferreira[c,f], S. C. Nunes[a,g], V. de Zea Bermudez[a,b,1]

[a] Department of Chemistry, University of Trás-os-Montes e Alto Douro, 5001-801 Vila Real, Portugal

[b] CQ-VR, University of Trás-os-Montes e Alto Douro, 5001-801 Vila Real, Portugal

[c] CICECO, Aveiro Institute of Materials, University of Aveiro, 3810-193 Aveiro, Portugal

[d] 3B's Research Group, Department of Polymer Engineering, University of Minho Headquarters of the European Institute of Excellence on Tissue Engineering and Regenerative Medicine Avepark – Parque de Ciência e Tecnologia Zona Industrial da Gandra, 4805-017 Barco GMR- Portugal

[e] Department of Chemistry, University of Minho, Gualtar, 4710-057 Braga, Portugal

[f] Department of Physics, University of Aveiro, 3810-193 Aveiro, Portugal

[g] CICS –Health Sciences Research Center and Chemistry Department, University of Beira Interior, 6201-001 Covilhã, Portugal

[1] **Corresponding author**. vbermude@utad.pt; **Tel.:** +351 259350253; fax: +351 259350480

Abstract

Organic/inorganic biohybrids composed of poly(ε-caprolactone) (PCL(530) chains (where 530 represents the average molecular weight of the chains in $gmol^{-1}$) covalently bonded to a siloxane network via urethane linkages and incorporating home-made protic ionic liquids (PILs) were investigated. The materials (H-PIL_X, where H represents the host hybrid matrix and X is the ratio of the mass of PIL per mass of organic precursor) were doped with two different concentrations of N-ethylimidazolium trifluoromethanesulfonate [EIm][TfO] and N-butylimidazolium trifluoromethanesulfonate [BIm][TfO]. The samples were processed as essentially amorphous transparent films thermally stable up to at least 200 °C. The highest conductivity value (4.3×10^{-5} S cm^{-1}) was measured for H-$[EIm][TfO]_{16.4}$ at 105 °C. This work emphasizes that performing Scanning Electron Microscopy (SEM)/Energy Dispersive X-ray Spectroscopy (EDS) measurements is mandatory to determine the morphology of IL-based electrolytes. In the case of the most concentrated [BIm][TfO]-doped hybrid this technique enabled the detection of segregated silica-rich circular micro-sized regions formed as a result of the hydrophobic interactions established between the bulky butyl chains of the $[BIm]^+$ cation and the PCL(530) chains of the host matrix.

Keywords: poly(ε-caprolactone)/siloxane hybrid, N-ethylimidazolium trifluoromethanesulfonate, N-butylimidazolium trifluoromethanesulfonate, structure, morphology, and ionic conductivity.

1. Introduction

Ionic liquids (ILs) are an emergent class of compounds composed of bulky organic cations and inorganic or organic anions, whose nature only depends on the imagination of the chemists [1] [1]. Current applications of ILs span from organic synthesis [1][2], catalysis [2][3], and extraction [3][4], to medicine [4][5], optics [5][6] and energy [6][7].

Among the unique properties exhibited by ILs two are particularly attractive for the development of electrolytes for electrochemical devices [8,9][8][9]: the high ionic conductivity and the wide electrochemical stability domain. Another benefit of the use of ILs in this context derives from the fact that their low toxicity, non-flammability and recyclability gives them the eco-friendly label [10,11][10,11].

ILs can be categorized into two sub-classes: aprotic ILs and protic ILs (PILs), whose cation holds a mobile proton [12,13] [1213]. In the last few years it has been recognized that PILs offer exciting new challenges for advances in fuel cell technology, especially for high temperature and water-independent operation [14-23] [14, 15, 16][17, 18, 19, 20, 21, 22,23]. The interest of PILs derives from the fact that display three very interesting features: (1) They are prone to participating actively in hydrogen bonding interactions; (2) They demonstrate fast proton conduction in the absence of moisture; (3) They show high activity for fuel cell electrode reactions.

Very recently, in the framework of an investigation devoted to the development of quasi-anhydrous polymer/siloxane hybrid electrolytes (also called ormolytes, organically modified silicate electrolytes) [24,25][24][25], we reported the incorporation of two PILs (N-ethylimidazolium trifluoromethanesulfonate [EIm][TfO] [15, 26][15, 26] and the home-made N-butylimidazolium trifluoromethanesulfonate [BIm][TfO] [27][27]) into a di-ureasil host matrix (d-U(2000)) [28][28] (Está repetida e

há várias; dois 27,dois 28, etc…). This hybrid host structure, prepared by the sol-gel method [29][29], includes poly(oxyethylene) (POE) chains (ca. 40 oxyethylene repeat units) linked to a siliceous network via urea cross-links. At certain [EIm][TfO] doping levels the corresponding ormolytes were practically anhydrous, thermally stable up to 200 °C and displayed good mechanical properties [26][26]. Similarly to what happened to the [EIm][TfO]-containing system, the [BIm][TfO]-doped d-U(2000)-based electrolytes exhibited attractive structural, thermal and mechanical properties which persisted four years after the materials synthesis [27][27]. After this long period of time, the quasi-anhydrous electrolytes remained amorphous, homogeneous, flexible, and thermally stable below 200 ºC [27][27]. This family of [BIm][TfO]-based di-ureasils yielded higher ionic conductivities than the [EIm][TfO]-based analogues (3.5×10^{-5} Scm^{-1} [27] and 7.6×10^{-6} Scm^{-1} [26] for X = 30 at room temperature, where X, in %, is the ratio of the mass of PIL per mass of organic precursor). The morphological study of the [BIm][TfO]-doped d-U(2000)-based electrolytes performed by means of Scanning Electron Microscopy (SEM)/Energy Dispersive X-ray Spectroscopy (EDS) demonstrated the fundamental role played by this technique in the detection of expelled PILs at the surface of the samples, dictating the need (or not) for washing procedures and thus avoiding misleading conductivity values [27].

Motivated by these very encouraging results, we have incorporated in the present work the same PILs into a different hybrid framework. The host structure chosen, also synthesized by the sol-gel process, comprises short segments of the poly(ε-caprolactone) biopolymer [30-34][3031323334], containing -C(=O)$(CH_2)_5$O)- repeat units, and abbreviated as PCL(530) (where 530 represents the average molecular weight in g mol^{-1}), bonded to a siliceous network through urethane linkages. The structure, thermal behavior and ionic conductivity of these two novel families of d-

PCL(530)/siloxane-based ormolytes have been characterized. The incorporation of ILs into this host matrix is of interest. Ormolytes comprising the same host framework and various ionic salts [35-40] [35,36,37,38,39,40], or a mixture of an ionic salt and an IL [41][41], have been extensively explored by our group over the last decade. Maximum ionic conductivity values at 36 ºC were obtained when d-PCL(530)/siloxane was doped with a mixture of lithium triflate and 1-ethyl-3-methyl imidazolium tetrafluoroborate (2.5×10^{-5} [41]) or just with 1-ethyl-3-methyl imidazolium tetrafluoroborate ([Emim][BF_4] (4×10^{-4} Scm^{-1} for X = 70 [41]).

2. Experimental

2.1. Materials

N-ethylimidazole (≥ 95 %Aldrich), N-butylimidazole (98 %, Aldrich), trifluoromethanesulfonic superacid (HTfO, Fluka, p.a.), dichloromethane (Fluka, p.a.), α,ω-hydroxyl poly(ε-caprolactone) (PCL(530), Fluka, average molecular weight 530 $gmol^{-1}$) and 3-isocyanatepropyltriethoxysilane (ICPTES, 97%, Fluka) were used as received. Ethanol (EtOH, Panreac, p. a.) and tetrahydrofuran (THF, Merck) were stored over molecular sieves. High purity distilled water was used in all experiments.

2.2. Synthesis of the PILs

The basis for the synthesis of the PILs is a neutralization reaction between a Brönsted base (proton acceptor) and a Brönsted acid (proton donor). The synthesis of the PILs employed in the current work was described in detail in previous works [14, 25, 26][15, 26, 27]. Briefly, to produce [EIm][TfO] and [BIm][TfO] the imidazole bases N-ethylimidazole and N-butylimidazole were mixed with an equivalent molar amount

of HTfO, respectively [13-15] [14,15,16]. The structure of the PILs was confirmed by ^{1}H NMR spectroscopy.

2.3. Synthesis of the ormolytes

The host d-PCL(530)/siloxane hybrid was produced according to the procedure reported elsewhere [34][35]. The synthetic procedure occurred in two steps. In the first stage a urethane cross-link was formed between the hydroxyl end groups of the PCL(530) chains and the isocyanate groups of ICPTES in THF at 50-60 ºC to yield the non-hydrolyzed d-PCL(530)/siloxane hybrid precursor. In the second stage appropriate amounts of EtOH and water were added to this solution to promote the hydrolysis and condensation reactions. [EIm][TfO] and [BIm][TfO] were incorporated in the latter stage. Details of the synthetic procedure are found in Table 1. Xerogels with two different PIL concentrations X were prepared. All the samples were obtained as highly transparent and flexible films. The materials were identified using the notation **H-PIL$_X$**, where H stands for d-PCL(530)/siloxane.

Table 1. Details of the synthesis of the **H-PIL$_X$** ormolytes.

PIL	X (%)	$m_{PCL(530)}$ (g)	V_{ICPTES} (mL)	m_{PIL} (g)	V_{H2O} (mL)	V_{EtOH} (mL)
[EIm][TfO]	16.4	0.5204	0.4888	0.0853	0.1060	0.4586
	5.7	0.5871	0.5469	0.0334	0.1196	0.5174
[BIm][TfO]	15.6	0.5714	0.5323	0.0890	0.1164	0.5036
	7.7	0.5179	0.4824	0.0400	0.1055	0.4554

2.4. Experimental characterization techniques

2.4.1. Thermogravimetric analysis (TGA)

For the TGA experiments the samples were transferred to open platinum crucibles and analysed from room temperature to 700 ºC using a TA Instruments Q50 thermobalance at a heating rate of 10 ºC min^{-1}. The purge gas used was high purity nitrogen (N_2) with a flow rate of 40 mL min^{-1} (balance gas) and 60 mL min^{-1} (sample gas).

2.4.2. Differential Scanning Calorimetry (DSC)

A DSC131 Setaram Differential Scanning Calorimeter was used to determine the thermal characteristics of the ormolytes. Disk sections with a mass of approximately 15 mg were removed from the ormolyte film and placed in 30 μl aluminum cans. After this the cans were hermetically sealed and stored in phosphorous pentoxide for one week before the thermograms were recorded. Each sample was heated from 25 to 90 ºC at 10 ºC min^{-1}. The purge gas used was high purity N_2 supplied at a constant 35 mLmin^{-1} flow rate.

2.4.3. X-ray diffraction (XRD)

XRD patterns were recorded at room temperature using a Rigaku Geigerflex D/max-c diffractometer system. The films were exposed to monochromated CuK_α radiation (λ = 1.54 Å) over the 2θ range between 3 and 60 º with a 2θ range resolution of 0.02 º.

2.4.4. SEM and EDS

SEM micrographs of **H-[EIm][TfO]$_{5.7}$** and **H-[EIm][TfO]$_{16.4}$** were recorded using a SEM/ESEM-FEI Quanta 400 equipment operating at a high acceleration voltage (25-30 kV) and also FEI QUANTA 400 FEG/EDAX Pegasus X4M (CEMUP-Porto, contracts REEQ/1062/CTM/2005 and REDE/1512/RME/2005 FCT). A small portion of the

sample was cut, fixed on an aluminium stub with carbon tape and then coated with Au/Pd. SEM images of **H-[BIm][TfO]$_{7.7}$** and **H-[BIm][TfO]$_{15.6}$** were obtained at 20 kV on a Hitachi S-3400N type II microscope equipped with a Bruker x-flash 5010 at high vacuum. The samples were coated with Au. Elemental mapping analysis on microscopic sections of selected electrolytes were performed by EDS. The acquisition time for satisfactory resolution and noise performance was 60 s.

2.4.5. Polarized Optical Microscopy (POM)

POM images were recorded using an OPTIKA B-600POL microscope equipped with a 8M pixel Digital Photo Camera. The images were analyzed using with the OPTIKA VISION PRO software.

2.4.6. Complex impedance measurements

Prior to characterization of conductivity behavior, the ormolytes were vacuum-dried at 80 ºC for about 48 h and stored in a high-integrity, argon-filled glove box. For bulk conductivity measurements, an ormolyte disk was placed between two 10 mm diameter ion blocking gold electrodes (Goodfellow, >99.9%). The electrode/ormolyte/electrode assembly was secured in a suitable constant-volume support, which was installed in a Buchi TO 51 tube oven. A calibrated type K thermocouple, placed close to the ormolyte disk, was used to measure the sample temperature with a precision of about ±0.2 ºC and samples were characterized over a temperature range of between 25 and 100 ºC. Bulk conductivities of the samples were obtained during heating cycles using the complex plane impedance technique (Schlumberger Solartron 1250 frequency response analyzer and 1286 electrochemical interface penso que na altura era este equipamento….mas tenho dúvidas, embora possamos deixar assim) over a frequency range of 65 kHz to 0.5

Hz. The electrolyte behavior was found to be almost ideal and bulk conductivities were extracted in the conventional manner from impedance data by using an equivalent circuit composed of R_b in parallel with C_g, where R_b is the electrical resistance of the electrolyte and C_g is its geometric capacity. The circuit element corresponding to the blocking electrode interface was simulated by a series C_{dl} element, where C_{dl} in the double layer capacity.

3. Results and discussion

3.1. Thermal, structural and morphological characterization

The TGA curve of the d-PCL(530)/siloxane biohybrid reproduced in Figure 1 (black line) shows that the decomposition of this xerogel is initiated at approximately 235 ºC [36][37]. **H-[EIm][TfO]$_{5.7}$** suffered a weight loss of 3 % below 300 ºC, with a subsequent abrupt loss of 60 % up to T < 466 ºC (Figure 1, blue line). At 700 ºC ca. 30 % of the initial mass had not been degraded. **H-[BIm][TfO]$_{7.7}$**, **H-[BIm][TfO]$_{15.6}$** and **H-[EIm][TfO]$_{16.4}$** yielded a similar thermal degradation pattern (Figure 1, red, magenta and cyanide lines, respectively). These three samples suffered a gradual weight loss of about 10 % between room temperature and ca. 310 ºC. After this temperature the weight losses were 64 % (T < 415 ºC), 60 % (T < 470 ºC) and 66 % (T < 430 ºC), respectively. At 700 ºC, about 17 and 30 % remained to be decomposed in the case of **H-[BIm][TfO]$_{7.7}$** and **H-[BIm][TfO]$_{15.6}$**, respectively, and 19 % in the case of **H-[EIm][TfO]$_{16.4}$**.

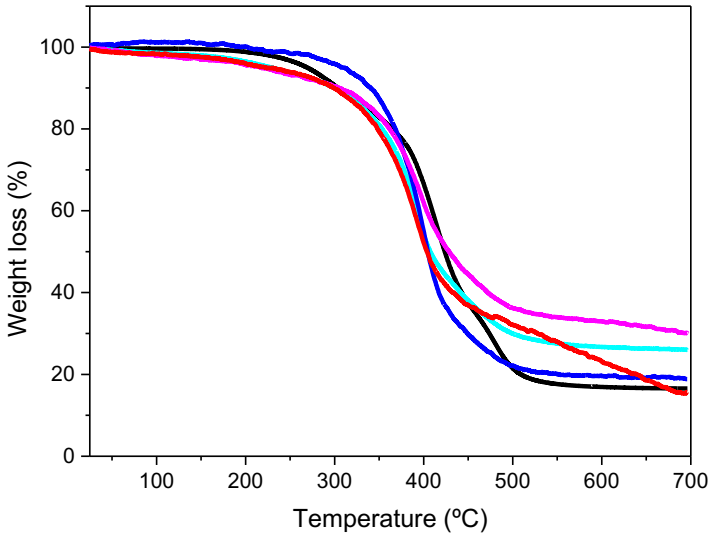

Figure 1. TGA curves of d-PCL(530)/siloxane (black line) [37] [37], **H-[EIm][TfO]$_{5.7}$** (blue line), **H-[EIm][TfO]$_{16.4}$** (cyanide line), **H-[BIm][TfO]$_{7.7}$** (red line) and **H-[BIm][TfO]$_{15.6}$** (magenta line).

The DSC curves of the [BIm][TfO]-based ormolytes revealed the disordered nature of these materials (Figure 2A). A predominantly amorphous character was also reported for the di-ureasil systems doped with [EIm][TfO] [25][26] and [BIm][TfO] [26][27]. In contrast, at the lowest concentration of [EIm][TfO] (X = 5.7) (Figure 2A, blue line) an endothermic peak centered at 46 ºC (onset at ca. 35 ºC) was observed. We also detected the presence of this thermal event in the DSC curves of some d-PCL(530)/siloxane-based ormolytes incorporating europium β-diketonate complexes [41][42], alkaline metal salts ~~[37]~~[37],[~~40~~][40], mixtures of alkaline and lanthanide metal salts [39][39], respectively), mixtures of an alkaline metal salt and an IL [41] and solely an IL [41][41]. This endotherm was attributed to the fusion of the short polymer segments of PCL(530) which should occur around 36-48 ºC. At higher [EIm][TfO] content (X = 16.4) (Figure 2A, cyanide line) the intensity of this peak, centered at 49 ºC (onset at

about 37 ºC), decreased. The degree of crystallinity calculated for **H-[EIm][TfO]$_{5.7}$** and **H-[EIm][TfO]$_{16.4}$** using the expression % crystallinity = $(\Delta H_f / \Delta H_m^0) \times 100$ (where ΔH_f is the enthalpy of fusion of the PCL chains derived from the DSC data (5.8 and 1.6 J g^{-1}, respectively) and ΔH_m^0 is the bulk enthalpy of melting of 100 % crystalline PCL (166.7 Jg^{-1} [42][43])) were 3.5 and 0.9 %, respectively, clearly suggesting that the samples were essentially amorphous.

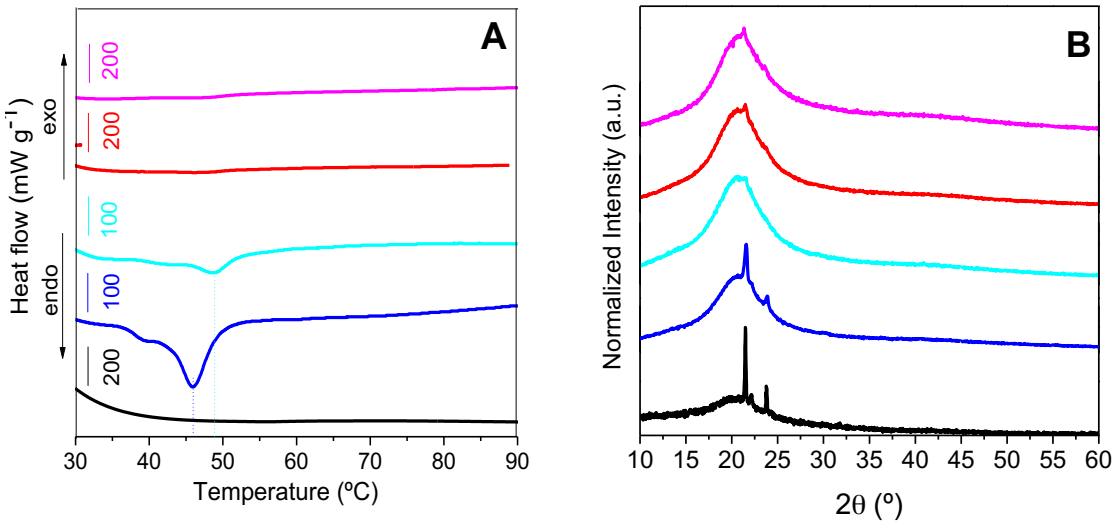

Figure 2. A: DSC curves of the d-PCL(530)/siloxane matrix (black line) [37] [37] and of the **H-[EIm][TfO]$_{5.7}$** (blue line), **H-[EIm][TfO]$_{16.4}$** (cyanide line), **H-[BIm][TfO]$_{7.7}$** (red line) and **H-[BIm][TfO]$_{15.6}$** (magenta line) ormolytes. B: XRD diffraction patterns of commercial PCL(530) (black line) and of the above indicated ormolytes.

The diffractograms of the doped samples and that of commercial PCL(530) (reproduced from reference [37][37] and normalized in the present work) are represented in Figure 2B. The characteristic Bragg peaks of commercial PCL(530) (Figure 2B, black line), located at ca. 21.5 and 23.8 ° [37][37], are also discerned in the case of **H- [EIm][TfO]$_{5.7}$** (Figure 2B, blue line). All the XRD patterns are characterized by a broad band, Gaussian in shape, centered at ca. 21.0 º, associated with ordering

within the siliceous network [42][44]. In the diffractograms of the samples doped with **[BIm][TfO]** the PCL(530) characteristic peaks at 21.5 and 23.8 º are slightly resolved in the broad band profile (Figure 2B, red and magenta lines). These results are in perfect agreement with the DSC data (Figure 2).

Figures 3(a)-3(c) show that the texture of **H-[EIm][TfO]$_{5.7}$**, homogeneous and irregular, did not differ significantly from that of the non-doped hybrid matrix [38][38]. The POM image obtained under crossed-polarizers, reproduced in the Inset of Figure 3(a), demonstrates that this sample exhibits sub-micrometric birefringence, as already observed for d-U(2000)[EIm][TfO]30 [25][26]. In the case of the more concentrated **H-[EIm][TfO]$_{16.4}$** sample, dispersed and irregular micro-sized aggregates were formed instead (Figures 3(d)-3(f)). This type of texture was also detected for the **H-[BIm]TfO]$_{7.7}$** hybrid (Figure 3(g)-3(j)). Figure 4 substantiates that the further incorporation of [BIm]TfO] into d-PCL(530)/siloxane had marked morphological consequences. The SEM image of Figure 4(a) shows that **H-[BIm]TfO]$_{15.6}$** yielded a quite interesting heterogeneous texture. The right top area reveals the existence of circular micro-objects with a diameter of about 20-50 μm, closely resembling water lily leaves, whereas the left bottom area points out, in addition, the presence of submicrometer objects located in the border of these round-shape formations. The quite unusual EDS mapping images represented in Figures 4(a1) and 4(b1) provide clear evidence that in **H-[BIm]TfO]$_{15.6}$** practically all the silicon atoms were confined to these objects. Also quite interesting is the fact that the boundaries of these micro-objects contained a high concentration of carbon atoms (Figures 4(a2) and 4(b2)). According to the EDS data, all the other atoms analyzed remained homogeneously distributed in the sample (Figures 4(a3)-4(a6) and 4(b3)-4(b6)). The same conclusions may be beautifully

drawn from the EDS spectra shown at the left and right top of Figure 4, associated with the SEM images of Figures 4(a) and 4(b), respectively.

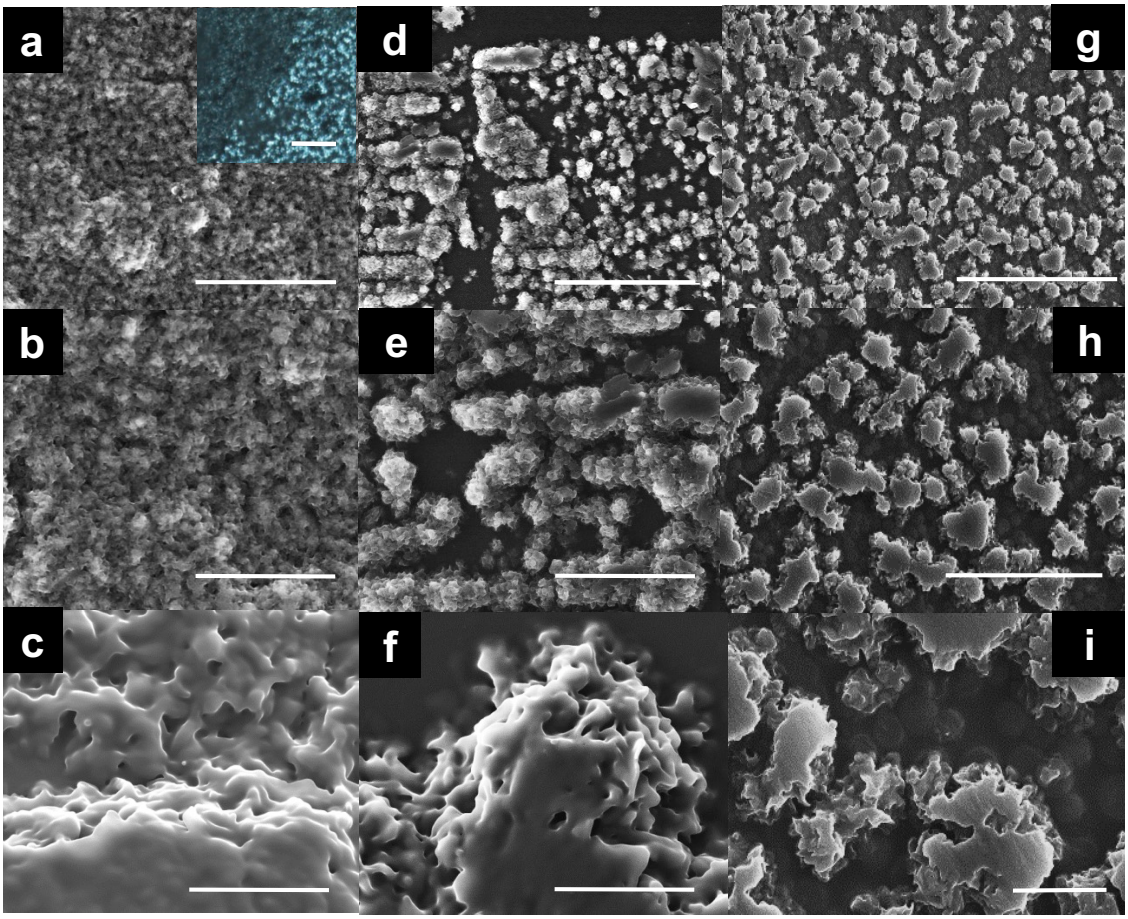

Figure 3. SEM images of the **H-[EIm][TfO]$_{5.7}$** (a, scale bar = 100 μm; b, scale bar = 50 μm; c, scale bar = 10 μm), **H-[EIm][TfO]$_{16.4}$** (d, scale bar = 100 μm; e, scale bar = 50 μm; f, scale bar = 10 μm) and **H-[BIm][TfO]$_{7.7}$** (g, scale bar = 100 μm; h, scale bar = 50 μm; i, scale bar = 10 μm) ormolytes. Inset of (a) shows a POM image obtained under crossed-polarizers.

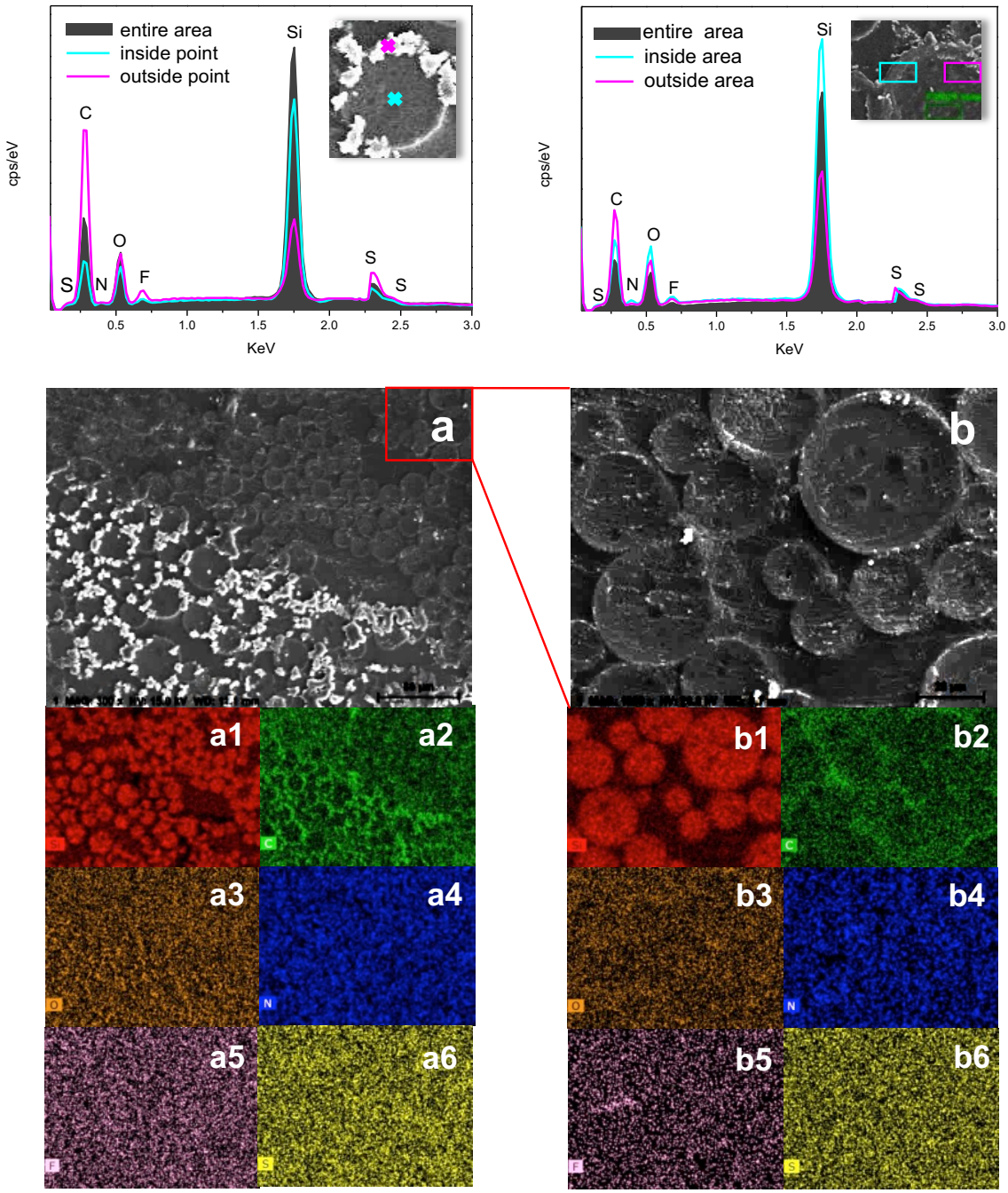

Figure 4. SEM images (a, scale bar = 80 μm; b, scale bar =20 μm) and EDS mapping images for silicon (a1, b1), carbon (a2, b2), oxygen (a3, b3), nitrogen (a4, b4), fluorine (a5, b5) and sulfur (a6, b6) atoms of the **H-[BIm][TfO]$_{15.6}$** ormolyte. Top: EDS spectra corresponding to selected points and areas of the SEM images (a) (left) and (b) (right).

Based on these results we are led to propose that the formation of the segregated silica-rich circular micro-objects found in the **H-[BIm]TfO]$_{15.6}$** material was due to the establishment of hydrophobic interactions between the butyl chains of the imidazolium ring of the $[BIm]^+$ ion and the PCL(530) chains. The high concentration of carbon atoms in the boundary of the silica regions gives strong support to this explanation. Scheme 1 shows a tentative explanation of the texture found in Figure 4(b). It is useful to recall at this stage that in the case of the d-U(2000)/[BIm][TfO]X analogues with X = 10 and 30 % isolated circular micro-objects were also detected [27]. However, the EDS data allowed us concluding that the composition of these regions lacked, in contrast, silicon atoms, being mainly composed of carbon, oxygen and fluorine atoms and a minor amount of nitrogen and sulfur atoms, hence supporting the presence of [BIm][TfO], hydrophilic POE chains and urea cross-links [27].

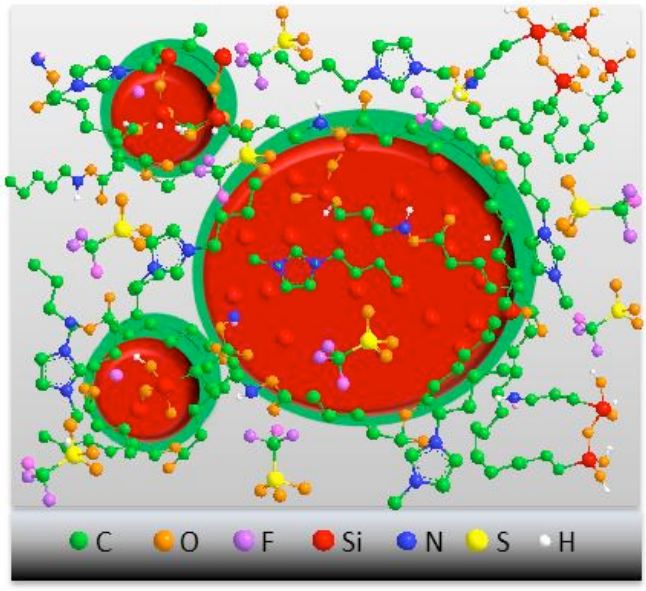

Scheme 1. Tentative representation of the chemical composition of the **H-[BIm][TfO]$_{15.6}$** ormolyte responsible for the morphology displayed in the SEM image of Figure 4(b) and in the EDS mapping images of Figure 4(b1)-4(b6).

(está muito bem esta figura! Adorei!)

3.2. Ionic conductivity

The Arrhenius conductivity plot of the **H-[PIL]$_X$** ormolytes and of selected d-U(2000)-based ormolytes incorporating similar concentrations of [EIm][TfO] [25] and **[**BIm][TfO] [26] shows that the **H-[PIL]$_X$** samples including [EIm][TfO] demonstrated higher ionic conductivity values than those containing [BIm][TfO] over the entire range of temperatures considered (Figure 5). This trend is opposed to that reported for the d-U(2000)-based di-ureasil electrolytes doped with [BIm][TfO] which exhibited higher conductivity [26][27] than those incorporating [EIm][TfO] [25][26]. In both **H-[PIL]$_X$** systems the ionic conductivity increased upon addition of more PIL, i.e,, of more charge carriers. In addition, the data of Figure 5 reveal that the ionic conductivity of the [EIm][TfO]- and [BIm][TfO]-doped ormolytes depend critically on the nature of the host polymer. The replacement of d-U(2000) by d-PCL(530)/siloxane was clearly disadvantageous. This was somehow expected, since the PCL(530) chains are considerable less flexible than the POE chains, which are known to play a major role in the ion conduction of PEs, promoting segmental motions which facilitate and assist the transport of the charge carriers [45].

The values obtained are too low to envisage any practical applications. (Acho que aqui poderiamos colocar que poderiam ser aplicados em dispositivos electrocromicos pois não necessitam de uma condutividade assim tão elevada e colocar algumas referências…Mariana envio uma ref. recente minha que com 10^{-7} a 30 ºC foi aplicado em janelas) alguns revisores implicam com as aplicações…..Only above 100 ºC did the **H-[EIm][TfO]$_X$** samples exhibit ionic conductivity values higher than the threshold value that dictates the feasibility of a material a electrolyte for electrochemical devices (10^{-5} Scm^{-1}) (Figure 5, blue and cyanide symbols, and Table 2) [46]. However, comparison with the IL concentration of the d-PCL(530)/siloxane ormolyte doped with

[Emim][BF_4] (X = 70.4), which exhibited significant ionic conductivity (0.4 and 2 mS cm^{-1} at 36 and 98 ºC, respectively), allows concluding that the PIL concentrations used in the present work are rather low.

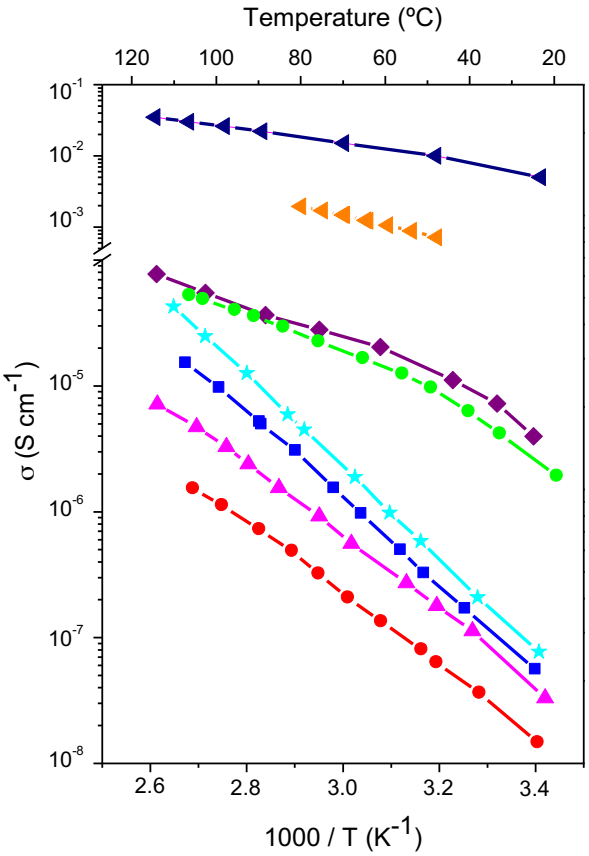

Figure 5. Arrhenius condutivity plots of [BIm][TfO] (orange symbols [27]), [EIm][TfO] (navy blue symbols [27]), d-U(2000)/[EIm][TfO]5 (green symbols [26]), d-U(2000)/[BIm][TfO]5 (purple symbols [27]) and of the **H-[EIm][TfO]$_{5.7}$** (blue symbols), **H-[EIm][TfO]$_{16.4}$** (cyanide symbols), **H-[BIm][TfO]$_{7.7}$** (red symbols) and **H-[BIm][TfO]$_{15.6}$** (magenta symbols) ormolytes.

Table 2. Ionic conductivity (σ) and activation energy (E_a) values determined from the slope of the Arrhenius plot of the **H-PIL$_X$** ormolytes.

PIL	X (%)	σ (S cm^{-1})		E_a (kJ mol^{-1}/eV)
		21 ºC	≈ 108 ºC	

[EIm][TfO]	16.4	7.7×10^{-8}	4.3×10^{-5}	69.8/4.35
	5.7	5.4×10^{-8}	1.5×10^{-5}	65.3/4.07
[BIm][TfO]	15.6	3.3×10^{-8}	7.2×10^{-6}	55.3/3.45
	7.7	1.5×10^{-8}	1.5×10^{-6}	54.2/3.38

The ionic conductivity of the **H-PIL$_X$** samples obeyed the Arrhenius equation $\sigma = \sigma_0 \exp(-E_a/RT)$ (where σ_0 is a pre-exponential factor, E_a is the activation energy, R is the gas constant and T is the temperature in K) yielding a straight line when plotted as the natural logarithm versus reciprocal temperature with regression values close to unity ($R^2 \sim 0.99$) (Figure 5, blue, cyanide, red and magenta symbols). This linear temperature dependence of the ionic conductivity indicates that the ion transport in the d-PCL(530)/siloxane-based electrolytes was thermally activated. This behaviour, which is typical in PEs where a hopping mechanism of ionic charge species dominates, contrasts with the non-linear variation reported for the d-U(2000)-based di-ureasil systems [26,27], in which chain mobility exerted an important role. The absence of sudden variations of ionic conductivity in the range of temperatures examined in the case of the **H-PIL$_X$** samples is in perfect agreement with the DSC and XRD data which pointed out their essentially amorphous nature. The increase of ionic conductivity that results from the increase of temperature is a well-known phenomenon. It is primarily associated with the vibrational energy of the segmental motion of the polymer chains that leads to the creation of free volume around them, thus facilitating the mobility of ions and favoring inter- and intra-chain ion hopping. As a result, the ionic conductivity of the polymer electrolyte becomes higher. The increase of ionic conductivity as a function of temperature may be also correlated with a decrease in the polymer viscosity and the concomitant increase in chain flexibility.

It is of interest to examine the E_a values calculated for the **H-PIL$_X$** samples from the slope of the Arrhenius plot (Table 2). The E_a is associated with the potential barrier to be overcome by the ions in order to hop from one site to another in the material, assuming that the host structure remains unchanged, plus the energy required to deform the structure to allow the migration of the ions. Curiously the E_a values of the **H-[BIm][TfO]$_X$** ormolytes are lower than those of the **H-[EIm][TfO]$_X$** analogues, although the latter samples are those which displayed the highest ionic conductivities. Moreover, while the E_a value of **H-[EIm][TfO]$_{5.7}$** increased slightly upon addition of more [EIm][TfO], in the case of the **H-[BIm][TfO]$_X$** materials E_a was practically independent of **[BIm][TfO]** concentration. The E_a values calculated in the present work for the **H-[EIm][TfO]$_X$** ormolytes are of the same order of magnitude of those reported for gelatin-based electrolytes doped with lithium perchlorate (62.7 kJ mol^{-1} [47]).

A Grotthus-like mechanism may be invoked to explain proton transport in the **H-[PIL]$_X$** ormolytes. Proton hopping involving the $[PIL]^+$ cations, the oxygen atoms of the ester groups and/or of the urethane carbonyl groups of the PCL(530) chains may have operated.

4. Conclusions

Essentially amorphous, transparent and flexible sol-gel derived di-urethane cross-linked PCL(530)/siloxane organic-inorganic biohybrid containing two PILs ([EIm][TfO] and [BIm][TfO]) (**H-PIL$_X$**, where H represents the host hybrid matrix and X, concentration, is the ratio of the mass of PIL per mass of organic precursor)) with X values similar to those employed previously in di-ureasil analogs [26,27] eu retirava as ref. das conclusões were investigated. The biohybrid doped with PIL analysed were produced as thin amorphous, flexible monoliths (está repetido …) with excellent thermal stability.

SEM/EDS data were essential to detect segregated silica-rich circular micro-sized regions in the most concentrated [BIm][TfO]-doped hybrid. These regions emerged as a result of the hydrophobic interactions established between the butyl chains of the $[BIm]^+$ cation and the PCL(530) chains of the host matrix. The ionic conductivity values exhibited by the **H-PIL$_X$** samples were considerably lower than those reported for the di-ureasil systems [26,27] eu retirava as ref. Best results were obtained in the presence of [EIm][TfO]. The H-[EIm][TfO]$_{5.7}$ hybrid displays the highest ionic conductivity over the range of temperatures analysed (approximately 5.4 x$\cdot 10^{-8}$ and 1.5 x$\cdot 10^{-5}$ S cm^{-1} at 21 and 108 ºC, respectively. The present work suggests that further investment in the **H-[EIm][TfO]$_X$** system is justified. Higher [EIm][TfO] concentrations must be considered in the future. Is important to refer that however, in commercial devices the ionic conductivity is undeniably of crucial importance, practical aspects of thermal, chemical and morphology behavior should not be ignored.

Acknowledgements

The work was supported by National Funds by FCT (Foundation for Science and Technology) and by FEDER funds through the POCI - COMPETE 2020 - Operational Programme Competitiveness and Internationalisation in Axis I - Strengthening research, technological development and innovation (UID/QUI/00616/2013, POCI-01-0145-FEDER-007491, UID/Multi/00709/2013, and LUMECD (POCI-01-0145-FEDER-016884 and PTDC/CTM-NAN/0956/2014) and UniRCell (SAICTPAC/0032/2015 and POCI-01-0145-FEDER-016422) projects). M. Fernandes, L.C. Rodrigues and M. A. Cardoso acknowledge FCT for grants (SFRH/BPD/78919/2011, XXXXXX and BII/UNI/0616/QUI/2009, respectively). S. C. Nunes acknowledges FCT for a for Post-PhD Fellowship of LUMECD project.

References

[1] Armand, M.; Endres, F. MacFarlane; D.R., Ohno H.; Scrosatei, B. Ionic liquid materials for the electrochemical challenges in the futire, *Nature Mater.***2009**, 621-629.

[2] *Ionic liquids in synthesis*, Wasserscheid, P.; Welton, T. (Eds.) Wiley-VCH, Weinheim, Germany, 2002.

[3] Sheldon, R. Catalytic reactions in ionic liquids, *Chem. Commun.* **2001**, 2399-2407.

[4] Huddleston, J.G.; Rogers, R.D. Room temperature ionic liquids as novel media for 'clean' liquid–liquid extraction, *Chem. Commun.* **1998**, 1765-1766.

[5] Smiglak, M.; Pringle, J.M.; Lu, X.; Han, L.; Zhang, S.; Gao, H.; MacFarlane, D.R.; Rogers, R.D. Ionic liquids for energy, materials, and medicine, *Chem. Commun.* **2014**, 50, 9228-9250.

[6] Bideau, J.L.; Viau, L.; Vioux, A. Ionogels, ionic liquid based hybrid materials, *Chem. Soc. Rev.* **2011**, 40, 907-925.

[7] MacFarlane, D.R.; Tachikawa, N.; Forsyth, M.; Pringle, J.M.; Howlett, P.C.; Elliott, G.D.; Davis Jr., J.H.; Watanabe, M.; Simon, P.; Angell, C.A. Energy applications of ionic liquids, *Energy Environ. Sci.* **2014**, 7, 232-250.

[8] Ohno, H. Electrochemical aspects of ionic liquids; John Wiley & Sons. New Jersey, USA, **2005**.

[9] Shaplov, A.S.; Marcilla, R.; Mercerreyes, D. Recent advances in innovative polymer electrolytes based on poly(ionic liquids), *Electrochim. Acta* **2015**, 175, 18-34.

[10] Petkovic, M.; Seddon K.R.; Rebelo, L.P.; Pereira, C.S. Ionic liquids: a pathway to environmental acceptability, *Chem. Soc. Rev.* **2011**, 40, 1383-1403.

[11] Ghandi, K. A review of ionic liquids, their limits and applications, *Green and Sustainable Chemistry* **2014**, 4, 44-53.

[12] Greaves, T.L.; Drummond, C.J. Protic ionic liquids: Properties and applications, *Chem. Rev.* **2008**, 108, 206–237.

[13] Greaves, T.L.; Drummond, C.J. Protic ionic liquids: Evolving structure-property relationships and expanding applications, *Chem. Rev.* **2015**, 115, 11379−11448.

[14] Fernicola, A.; Panero, S.; Scrosati, B.; Tamada, M.; Ohno, H. New types of Brönsted acid–base ionic liquids-based membranes for applications in PEMFCs, *Chem. Phys. Chem.* **2007**, 8, 1103-1107.

[15] Yan, F.; Yu, S.; Zhang, X.; Qiu, L.; Chu, F.; You, J.; Lu, J. Enhanced proton conduction in polymer electrolyte membranes as synthesized by polymerization of protic ionic liquid-based microemulsions, *Chem. Mater.* **2009**, 21, 1480-1484.

[16] Lin, B.; Cheng, S.; Qiu, L.; Yan, F.; Shang, S.; Lu, J. Protic ionic liquid-based hybrid proton-conducting membranes for anhydrous proton exchange membrane application, *Chem. Mater.* **2010**, 22, 1807-1813.

[17] Matsuoka, H.; Nakamoto, H.; Susan, Md.A.B.H.; Watanabe, M. Brönsted acid-base and -polybase complexes as electrolytes for fuel cells under non-humidifying conditions, *Electrochim. Acta* **2005**, 50, 4015-4021.

[18] Nakamoto, H.; Noda, A.; Hayamizu, K.; Hayashi, S.; Hamaguchi, H.-o; Watanabe, M. Proton-conducting properties of a Brønsted acid−base ionic liquid and ionic melts consisting of bis(trifluoromethanesulfonyl)imide and benzimidazole for fuel cell electrolytes, *J. Phys. Chem. C* **2007**, 111, 1541-1548.

[19] Nakamoto, H.; Watanabe, M. Brönsted acid-base ionic liquids for fuel cell electrolytes, *Chem. Commun.* **2007**, 2539-2541.

[20] Lee, S.-Y.; Ogawa, A.; Kanno, M.; Nakamoto, H.; Yasuda, T.; Watanabe, M. Nonhumidifed intermediate temperature fuel cells using protic ionic liquids, *J. Amer. Chem. Soc.* **2010**, 132, 9764-9773.

[21] Ueno, K.; Tokuda, H.; Watanabe, M. Ionicity in ionic liquids: correlation with ionic structure and physicochemical properties, *Phys. Chem. Chem. Phys.* **2010**, 12, 1649-1658.

[22] Lee, S.-Y.; Yasuda, T.; Watanabe, M. Fabrication of protic ionic liquid/sulfonated polyimide composite membranes for non-humidified fuel cells, *J. Power Sources* **2010**, 195, 5909-5914.

[23] Miran, M.S.; Kinoshita, H.; Yasuda, T.; Susan, Md.A.B.H.; Watanabe, M. Physicochemical properties determined by ΔpK_a for protic ionic liquids based on an organic super-strong base with various Brönsted acids, *Phys. Chem. Chem. Phys.* **2012**, 14, 5178-5186.

[24] *Functional hybrid materials*; Gomez-Romero, P.; Sanchez, C. (Eds.), Wiley Interscience, New York, USA, **2003**.

[25] Laberty-Robert, C.; Vallé, K.; Pereira, F.; Sanchez, C. Design and properties of functional hybrid organic-inorganic membranes for fuel cells, *Chem. Soc. Rev.* **2011**, 40, 961-1005.

[26] Cardoso, M.A; Fernandes, M.; Rodrigues, L.C.; Leones, R.; Silva, M.M.; de Zea Bermudez, V. Quasi-anhydrous proton conducting di-ureasil hybrid electrolytes incorporating a protic ionic liquid, *Electrochim. Acta* **2014**, 147, 288-293.

[27] Cardoso, M.A.; Leones, R.; Rodrigues, L.C.; Fernandes, M.; Figueiredo, F.L.; Nunes, S.C.; Silva, M.M.; de Zea Bermudez, V. Di-ureasil hybrid electrolytes incorporating a new proton ionic liquid, *ChemElectroChem* **2016**, 3, 783-789.

[28] de Zea Bermudez, V.; Carlos, L. D.; Alcácer, L. Sol-gel derived urea cross-linked organically modified silicates. 1. Room temperature mid-infrared spectra, *Chem. Mater.* **1999,** 11*,* 569-580.

[29] *Sol-gel Sscience: The physics and chemistry of sol-gel processing*, Brinker, C.J.; Scherer, G.W. (Eds.) Academic Press, San Diego, USA, **1990**.

[30] Woodruff, M.A.; Hutmacher, D.W. The return of a forgotten polymer-Polycaprolactone in the 21st century, *Prog. Polym. Sci.* **2010**, 35, 1217-1256.

[31] Labet, M.; Thielemans, W. Synthesis of polycaprolactone: a review, *Chem. Soc. Rev.* **2009**, 38, 3484-3504.

[32] Lam, C.X.; Teoh, S.H.; Hutmacher, D.W. Comparison of the degradation of polycaprolactone and polycaprolactone-(β-tricalcium phosphate) scaffolds in alkaline medium, *Polym Int.* **2007**, 56, 718–728.

[33] Abedalwafa, M.; Wang, F.; Wang, L.; Li, C. Biodegradable poly-epsilon-caprolactone (PCL) for tissue engineering aplications: a review, *Rev. Adv. Mater. Sci.* **2013**, 34, 123-140.

[34] Beltran, A.; Valente, A.J.M.; Jimeńez, A.; Garrigos, M.C. Characterization of poly(ε-caprolactone)-based nanocomposites containing hydroxyltyrosol for active food packaging, *J. Agric. Food Chem.* **2014**, 62, 2244-2252.

[35] Nunes, S.C.; de Zea Bermudez, V.; Silva, M.M.; Smith, M.J.; Morales, E.; Carlos, L.D.; Ferreira, R.A.S.; Rocha, J. Sol-gel derived Li^{+}-doped poly(ε-caprolactone)/siloxane biohybrid electrolytes, *J. Solid State Electrochem.* **2006**, 10, 203-210.

[36] Teixeira, J., Fernandes, M.; de Zea Bermudez, V; Rodrigues, L.C.; Silva, M.M.; Smith, M.J. Mg^{2+}-doped poly(ε-caprolactone)/siloxane biohybrids, *Electrochim. Acta* **2010**, 55, 1328-1332.

[37] Fernandes, M.; Rodrigues, L.C.; Ferreira, R.A.S.; Gonçalves, A.; Fortunato, E.; Silva, M.M.; Smith, M.J.; Carlos, L.D.; de Zea Bermudez, V. K^{+}-doped poly(ε-

caprolactone)/siloxane biohybrid electrolytes for electrochromic devices, *Solid State Ionics* **2011**, 204-205, 129-139.

[38] Fernandes, M.; Nobre, S.S.; Rodrigues, L.C.; Gonçalves, A.; Rego, R.; Oliveira, M.C.; Ferreira, R.A.S.; Silva, M.M.; Fortunato, E.; Carlos, L.D.; de Zea Bermudez, V. Li^{+}- and Eu^{3+}-doped poly(ε-caprolactone)/siloxane biohybrid electrolytes for electrochromic devices, *ACS Appl. Mater. Interfaces* **2011**, 3, 2953–2965.

[39] Fernandes, M.; Freitas, V.T.; Pereira, S.; Fortunato, E.; Ferreira, R.A.S.; Carlos, L.D.; Rego, R.; de Zea Bermudez, V. Green Li^{+}- and Er^{3+}-doped poly(ε-caprolactone)/siloxane biohybrid electrolytes for smart electrochromic windows, *Sol. Energy Mater. Sol. Cells* **2014**, 13, 203-210.

[40] Fernandes, M.; Leones, R.; Pereira, S.; Costa, A.M.S.; Mano, J.F.; Silva, M.M.; Fortunato, E.; de Zea Bermudez, V.; Rego, R. Eco-friendly sol-gel derived sodium-based ormolytes for electrochromic devices, *Electrochim. Acta*, in press.

[41] Fernandes, M.; Leones, R.; Costa, A.M.S.; Silva, M.M.; Pereira, S.; Mano, J.; Fortunato, E.; Rego, R.; de Zea Bermudez, V. Electrochromic devices incorporating biohybrid electrolytes doped with a lithium salt, an ionic liquid or a mixture of both, *Electrochim. Acta* **2015**, 161, 226-235.

[42] Fernandes, M.; de Zea Bermudez, V.; Sá Ferreira, R.A.; Carlos, L.D.; Charas, A.; Morgado, J.; Silva, M.M.; Smith, M.J. Highly photostable luminescent poly(ε-caprolactone)siloxane biohybrids doped with europium complexes, *Chem. Mater.* **2007**, 19, 3892-3901.

[43] Chen, H.L.; Li, L.-J.; Lin, T.-L. Formation of segregation morphology in crystalline/amorphous polymer blends: Molecular weight effect, *Macromolecules* **1998**, 31, 2255-2264.

[44] Carlos, L.D.; de Zea Bermudez, V.; Sá Ferreira, R.A.; Marques, L.; Assunção, M. Sol-gel derived urea cross-linked organically modified silicates. 2. Blue-light emission, *Chem. Mater.* **1999**, 11, 581-588.

[45] Armand, M.; Chabagno, J.M.; Duclot M. in Extended Abstracts Second International Conference on Solid Electrolytes, St. Andrews, Volume 5, **1978**.

[46] Gray, F.M., Polymer Electrolytes, "RSC Materials. Monographs", Royal Society of Chemistry,. Cambridge, U.K., **1997**.

[47] Mattos, R.I.; Pawlicka, A.; Tambelli, C.E.; Donoso, J.P. NMR and Conductivity Study of Gelatin-Based Polymer ElectrolyteMol. Cryst. Liq. Cryst., 483, 2008, 120-129.

(referências automáticas, para apagar no fim)

---

1 Armand, M.; Endres, F. MacFarlane; D.R., Ohno H.; Scrosatei, B. Ionic liquid materials for the electrochemical challenges in the futire, *Nature Mater.***2009**, 621-629.

2 *Ionic liquids in synthesis*, Wasserscheid, P.; Welton, T. (Eds.) Wiley-VCH, Weinheim, Germany, **2002**.

3 Sheldon, R. Catalytic reactions in ionic liquids, *Chem. Commun.* **2001**, 2399-2407.

4 Huddleston, J.G.; Rogers, R.D. Room temperature ionic liquids as novel media for 'clean' liquid–liquid extraction, *Chem. Commun.* **1998**, 1765-1766.

5 Smiglak, M.; Pringle, J.M.; Lu, X.; Han, L.; Zhang, S.; Gao, H.; MacFarlane, D.R.; Rogers, R.D. Ionic liquids for energy, materials, and medicine, *Chem. Commun.* **2014**, 50, 9228-9250.

6 Bideau, J.L.; Viau, L.; Vioux, A. Ionogels, ionic liquid based hybrid materials, *Chem. Soc. Rev.* **2011**, 40, 907-925.

7 MacFarlane, D.R.; Tachikawa, N.; Forsyth, M.; Pringle, J.M.; Howlett, P.C.; Elliott, G.D.; Davis Jr., J.H.; Watanabe, M.; Simonf, P.; Angell, C.A. Energy applications of ionic liquids, *Energy Environ. Sci.* **2014**, 7, 232-250.

8 Ohno, H. *Electrochemical aspects of ionic liquids*; John Wiley & Sons. New Jersey, USA, 2005.

9 Shaplov, A.S.; Marcilla, R.; Mercerreyes, D. Recent advances in innovative polymer electrolytes based on poly(ionic liquids), *Electrochim. Acta* **2015**, 175, 18-34.

10 Petkovic, M.; Seddon K.R.; Rebelo, L.P.; Pereira, C.S. Ionic liquids: a pathway to environmental acceptability, *Chem. Soc. Rev.* **2011**, 40, 1383-1403.

11 Ghandi, K. A review of ionic liquids, their limits and applications, *Green and Sustainable Chemistry* **2014**, 4, 44-53.

12 Greaves, T.L.; Drummond, C.J. Protic ionic liquids: Properties and applications, *Chem. Rev.* **2008**, 108, 206–237.

13 Greaves, T.L.; Drummond, C.J. Protic ionic liquids: Evolving structure-property relationships and expanding applications, *Chem. Rev.* **2015**, 115, 11379−11448.

14 Fernicola, A.; Panero, S.; Scrosati, B.; Tamada, M.; Ohno, H. New types of Brönsted acid–base ionic liquids-based membranes for applications in PEMFCs, *Chem. Phys. Chem.*, **2007**, 8, 1103-1107.

15 Yan, F.; Yu, S.; Zhang, X.; Qiu, L.; Chu, F.; You, J.; Lu, J. Enhanced proton conduction in polymer electrolyte membranes as synthesized by polymerization of protic ionic liquid-based microemulsions, *Chem. Mater.* **2009**, 21, 1480-1484.

16 Lin, B.; Cheng, S.; Qiu, L.; Yan, F.; Shang, S.; Lu, J. Protic ionic liquid-based hybrid proton-conducting membranes for anhydrous proton exchange membrane application, *Chem. Mater.* **2010**, 22, 1807-1813.

17 Matsuoka, H.; Nakamoto, H.; Susan, Md.A.B.H.; Watanabe, M. Brönsted acid-base and -polybase complexes as electrolytes for fuel cells under non-humidifying conditions, *Electrochim. Acta* **2005**, 50, 4015-4021.

18 Nakamoto, H.; Noda, A.; Hayamizu, K.; Hayashi, S.; Hamaguchi, H.-o; Watanabe, M. Proton-conducting properties of a Brønsted acid−base ionic liquid and ionic melts consisting of bis(trifluoromethanesulfonyl)imide and benzimidazole for fuel cell electrolytes, *J. Phys. Chem. C* **2007**, 111, 1541-1548.

19 Nakamoto, H.; Watanabe, M. Brönsted acid-base ionic liquids for fuel cell electrolytes, *Chem. Commun.* **2007**, 2539-2541.

20 Lee, S.-Y.; Ogawa, A.; Kanno, M.; Nakamoto, H.; Yasuda, T.; Watanabe, M. Nonhumidifed intermediate temperature fuel cells using protic ionic liquids, *J. Amer. Chem. Soc.* **2010**, 132, 9764-9773.

21 Ueno, K.; Tokuda, H.; Watanabe, M. Ionicity in ionic liquids: correlation with ionic structure and physicochemical properties, *Phys. Chem. Chem. Phys.* **2010**, 12, 1649-1658.

22 Lee, S.-Y.; Yasuda, T.; Watanabe, M. Fabrication of protic ionic liquid/sulfonated polyimide composite membranes for non-humidified fuel cells, *J. Power Sources* **2010**, 195, 5909-5914.

23 Miran, M.S.; Kinoshita, H.; Yasuda, T.; Susan, Md.A.B.H.; Watanabe, M. Physicochemical properties determined by ΔpK_a for protic ionic liquids based on an organic super-strong base with various Brönsted acids, *Phys. Chem. Chem. Phys.* **2012**, 14, 5178-5186.

24 *Functional hybrid materials*; Gomez-Romero, P.; Sanchez, C. (Eds.), Wiley Interscience, New York, USA, **2003**.

25 Laberty-Robert, C.; Vallé, K.; Pereira, F.; Sanchez, C. Design and properties of functional hybrid organic-inorganic membranes for fuel cells, *Chem. Soc. Rev.* **2011**, 40, 961-1005.

26 Cardoso, M.A.; Fernandes, M.; Rodrigues, L.C.; Leones, R.; Silva, M.M.; de Zea Bermudez, V. Quasi-anhydrous proton conducting di-ureasil hybrid electrolytes incorporating a protic ionic liquid, *Electrochim. Acta* **2014**, 147, 288-293.

27 Cardoso, M.A.; Leones, R.; Rodrigues, L.C.; Fernandes, M.; Figueiredo, F.L.; Nunes, S.C.; Silva, M.M.; de Zea Bermudez, V. Di-ureasil hybrid electrolytes incorporating a new proton ionic liquid, *ChemElectroChem* **2016**, 3, 783-789.

28 de Zea Bermudez, V.; Carlos, L. D.; Alcácer, L. Sol-gel derived urea cross-linked organically modified silicates. 1. Room temperature mid-infrared spectra, *Chem. Mater.* **1999,** 11, 569-580.

29 *Sol-gel Sscience: The physics and chemistry of sol-gel processing*, Brinker, C.J.; Scherer, G.W. (Eds.) Academic Press, San Diego, USA, **1990**.

30 Woodruff, M.A.; Hutmacher, D.W. The return of a forgotten polymer-Polycaprolactone in the 21st century, *Prog. Polym. Sci.* **2010**, 35, 1217-1256.

31 Labet, M.; Thielemans, W. Synthesis of polycaprolactone: a review, *Chem. Soc. Rev.* **2009**, 38, 3484-3504.

32 Lam, C.X.; Teoh, S.H.; Hutmacher, D.W. Comparison of the degradation of polycaprolactone and polycaprolactone-(β-tricalcium phosphate) scaffolds in alkaline medium, *Polym Int.* **2007**, 56, 718–728.

33 Abedalwafa, M.; Wang, F.; Wang, L.; Li, C. Biodegradable poly-epsilon-caprolactone (PCL) for tissue engineering aplications: a review, *Rev. Adv. Mater. Sci.* **2013**, 34, 123-140.

34 Beltran, A.; Valente, A.J.M.; Jimeńez, A.; Garrigos, M.C. Characterization of poly(ε-caprolactone)-based nanocomposites containing hydroxyltyrosol for active food packaging, *J. Agric. Food Chem.* **2014**, 62, 2244-2252.

35 Nunes, S.C.;de Zea Bermudez, V.; Silva, M.M.; Smith, M.J.; Morales, E.; Carlos, L.D.; Ferreira, R.A.S.; Rocha, J. Sol-gel derived Li^{+}-doped poly(ε-caprolactone)/siloxane biohybrid electrolytes, *J. Solid State Electrochem.* **2006**, 10, 203-210.

36 Teixeira, J., Fernandes, M.; de Zea Bermudez, V.; Rodrigues, L.C.; Silva, M.M.; Smith, M.J. Mg^{2+}-doped poly(ε-caprolactone)/siloxane biohybrids, *Electrochim. Acta*, **2010**, 55, 1328-1332.

37 Fernandes, M.; Rodrigues, L.C.; Ferreira, R.A.S.; Gonçalves, A.; Fortunato, E.; Silva, M.M.; Smith, M.J.; Carlos, L.D.; de Zea Bermudez, V. K^{+}-doped poly(ε-

caprolactone)/siloxane biohybrid electrolytes for electrochromic devices, *Solid State Ionics* **2011**, 204-205, 129-139.

38 Fernandes, M.; Nobre, S.S.; Rodrigues, L.C.; Gonçalves, A.; Rego, R.; Oliveira, M.C.; Ferreira, R.A.S.; Silva, M.M.; Fortunato, E.; Carlos, L.D.; de Zea Bermudez, V. Li^{+}- and Eu^{3+}-doped poly(ε-caprolactone)/siloxane biohybrid electrolytes for electrochromic devices, *ACS Appl. Mater. Interfaces* **2011**, 3, 2953–2965.

39 Fernandes, M.; Freitas, V.T.; Pereira, S.; Fortunato, E.; Ferreira, R.A.S.; Carlos, L.D.; Rego, R.; de Zea Bermudez, V. Green Li^{+}- and Er^{3+}-doped poly(ε-caprolactone)/siloxane biohybrid electrolytes for smart electrochromic windows, *Sol. Energy Mater. Sol. Cells* **2014**, 13, 203-210.

40 Fernandes, M.; Leones, R.; Pereira, S.; Costa, A.M.S.; Mano, J.F.; Silva, M.M.; Fortunato, E.; de Zea Bermudez, V.; Rego, R. Eco-friendly sol-gel derived sodium-based ormolytes for electrochromic devices, *Electrochim. Acta*, in press.

41 Fernandes, M.; Leones, R.; Costa, A.M.S.; Silva, M.M.; Pereira, S.; Mano, J.; Fortunato, E.; Rego, R.; de Zea Bermudez, V. Electrochromic devices incorporating biohybrid electrolytes doped with a lithium salt, an ionic liquid or a mixture of both, *Electrochim. Acta* **2015**, 161, 226-235.

42 Fernandes, M.; de Zea Bermudez, V.; Sá Ferreira, R.A.; Carlos, L.D.; Charas, A.; Morgado, J.; Silva, M.M.; Smith, M.J. Highly photostable luminescent poly(ε–caprolactone)siloxane biohybrids doped with europium complexes, *Chem. Mater*. 2007, 19, 3892-3901.

43 Chen, H.L. ; Li, L.-J.; Lin, T.-L. Formation of segregation morphology in crystalline/amorphous polymer blends: Molecular weight effect, *Macromolecules* **1998**, 31, 2255-2264.

44 Carlos, L.D.; de Zea Bermudez, V.; Sá Ferreira, R.A.; Marques, L.; Assunção, M. Sol-gel derived urea cross-linked organically modified silicates. 2. Blue-light emission, *Chem. Mater.* **1999**, 11, 581-588.

45 Gray, F.M., Polymer Electrolytes, "RSC Materials. Monographs", Royal Society of Chemistry,. Cambridge, U.K., 1997.

46 M. Armand, J. M. Chabagno, M. Duclot, in Extended Abstracts Second International Conference on Solid Electrolytes, St. Andrews, Volume 5, 1978.

47 Mattos, R.I.; Pawlicka, A.; Tambelli, C.E.; Donoso, J.P. NMR and Conductivity Study of Gelatin-Based Polymer Electrolyte*Mol. Cryst. Liq. Cryst*., 483, **2008**, 120-129.